

Soft X-ray emission lines from photoionized accretion discs: constraints on their strength and width

D. R. Ballantyne^{1*}, R. R. Ross² and A. C. Fabian¹

¹*Institute of Astronomy, Madingley Road, Cambridge CB3 0HA*

²*Physics Department, College of the Holy Cross, Worcester, MA 01610, USA*

29 October 2018

ABSTRACT

We consider the properties of soft X-ray emission lines in the reprocessed emission from a photoionized accretion disc. Observations of these lines will be important in determining the ionization state and metallicity of the innermost regions of active galaxies. Calculations of reflection from a constant-density disc with an ionization parameter, ξ , between 250 and 1000 erg cm s⁻¹ show that emission from O VIII Ly α will dominate the soft X-ray emission spectrum. There is also significant emission from C VI, N VII, O VII, as well as Fe XVII–XIX. As ξ is increased these lines become weaker and are broadened by Compton scattering. Significantly increasing the O abundance primarily strengthens the O VII line, making it as large or larger than the O VIII line. The nitrogen and carbon lines are quite weak with equivalent widths (EWs) <30 eV, even with an increase in the N abundance. A hydrostatic ionized disc model has a more realistic density structure and shows a similar spectrum, but with the lines weaker and broader. This is a result of the hot ionized skin at the surface of the disc. We apply these results to the controversial claim of soft X-ray relativistic lines in the *XMM-Newton* spectrum of MCG–6–30–15. We are unable to find a situation where O VIII has the required EW without substantial emission from O VII. Furthermore, Compton scattering results in the blue wing of the O VIII line to be much broader than the \ll 10 eV drop observed in the data. We conclude that soft X-ray accretion disc lines will, in general, be weak and broad features and are unlikely to produce sharp edges in the data.

Key words: radiative transfer – galaxies: active – X-rays: galaxies – X-rays: general – galaxies: individual: MCG–6–30–15 – line: formation

1 INTRODUCTION

Features observed in the hard X-ray spectra of active galactic nuclei (AGN) are one of the most direct probes of the structure of accretion discs close to the central black hole. The prominent iron K α emission line at 6.4 keV and Compton hump at \sim 20–30 keV in the spectra of many Seyfert 1 galaxies indicates that optically thick material is being illuminated by the hard X-ray source (Pounds et al. 1990). As pointed out by Fabian et al. (1989), if this reflected emission arose from the accretion disc, then relativistic and Doppler effects would broaden the emission lines in a characteristic way. Observations of such a line allows a determination of not only the accretion disc structure close to the black hole, but also the space-time geometry in the strong gravity regime. The *ASCA* observatory (1993–2001) finally provided the sensitivity to search for relativistically broadened Fe K α lines, and detected a clear example in the spectrum of the bright Seyfert 1 galaxy MCG–6–30–15 (Tanaka et al. 1995). Since that initial discovery, broad Fe K α lines have been found in many other Seyferts (Nandra et al. 1997; Yaqoob et

al. 2002), and are now an integral part of AGN phenomenology (Fabian et al. 2000).

Calculations of the reprocessed emission from an irradiated slab of gas have shown that the Fe K α line, by virtue of its large fluorescent yield and relatively high cosmic abundance, is the strongest line in the reflection spectrum (George & Fabian 1991; Matt, Perola & Piro 1991). Yet, strong lines from abundant elements such as carbon, nitrogen and oxygen are also present at lower energies, and, if detected, would provide further information on the ionization state of the accretion disc. Models of reflection from photoionized discs have shown that the soft X-ray features are very sensitive to the ionization parameter of the disc material (Ross & Fabian 1993; Ross, Fabian & Young 1999). Determining the ionization state of the disc would constrain the magnitude of the illuminating radiation, and would therefore place limits on the amount of accretion energy that is released in the corona.

Although the soft X-ray spectra of Seyfert galaxies are complicated by features such as warm absorbers and soft excesses, the sensitivity and resolution provided by the instruments on board *XMM-Newton* and *Chandra* could allow relativistic soft X-ray emission lines to be found amongst the clutter and noise. Indeed,

* drb@ast.cam.ac.uk

claims of such lines from hydrogenic carbon, nitrogen and oxygen have already been made based on *XMM-Newton* Reflection Grating Spectrometer (RGS) spectra of MCG–6–30–15 and Mrk 766 (Branduardi-Raymont et al. 2001; Sako et al. 2002). Clearly, the time is right for a closer look at the properties of the soft X-ray accretion disc lines.

Here, we employ detailed models of photoionized accretion discs to investigate the properties (specifically, the strength and width) of the C, N & O lines found in the reflection spectra. A range of ionization parameters are considered, and both constant density slabs and hydrostatic atmospheres are used for the disc structure. The calculations and assumptions are outlined in the following section, with the results presented in Section 3. Finally, we discuss the implications of our results in light of the recent *XMM-Newton* observations and draw conclusions in Section 4.

2 COMPUTATIONS

Models of illuminated accretion discs have greatly increased in sophistication over the last couple of years. Initially, the calculations had assumed that the surface of the disc was a constant density slab (Ross & Fabian 1993; Życki et al. 1994; Magdziarz & Zdziarski 1995; Ross et al. 1999), and so the resulting gas structure and reflection spectrum could be characterized by the ionization parameter

$$\xi = \frac{4\pi F_X}{n_H}, \quad (1)$$

where F_X is the X-ray flux incident on the slab, and n_H is the hydrogen number density of the material. While such a simple structure has some theoretical justification (a standard optically-thick disc has a roughly constant vertical density profile in the radiation pressure dominated limit; Shakura & Sunyaev 1973), the heated surface of the slab was out of pressure equilibrium with the remainder of the material. Recently, more realistic calculations were performed with the surface of the disc required to remain in hydrostatic balance (Nayakshin, Kazanas & Kallman 2000; Ballantyne, Ross & Fabian 2001). Under this condition, the irradiated gas takes on a more ‘two-phase’ structure with an outer hot (\approx Compton temperature), ionized layer in pressure balance with a denser, colder and more neutral inner zone. The spectral features in the reflection spectra depend on the sharpness of the transition between the two layers (Nayakshin et al. 2000; Ballantyne & Ross 2002), but qualitatively appear to be a diluted version of the constant density models.

In this section, we detail ionized disc calculations made with both the constant density code of Ross & Fabian (1993) and the hydrostatic code of Ballantyne et al. (2001). Since these latter models are dependent on the unknown accretion disc parameters, this paper concentrates on the results from the constant density models. However, an example hydrostatic calculation will be shown to illustrate the similarities and differences between the two approaches.

Important updates were made to both codes in order to better determine the soft X-ray emission spectrum. First, more elements were treated, and more recombined ions of each element were included. This was necessary so that nitrogen lines would be included in the output spectrum and so that the opacity would be treated accurately throughout the soft X-ray portion of the spectrum. In addition to fully-ionized species, the following ions are included in the calculations: C III–VI, N III–VII, O III–VIII, Ne III–X, Mg III–XII, Si IV–XIV, S IV–XVI and Fe VI–XXVI. Details of the atomic physics used will be presented in a subsequent paper. Second, the

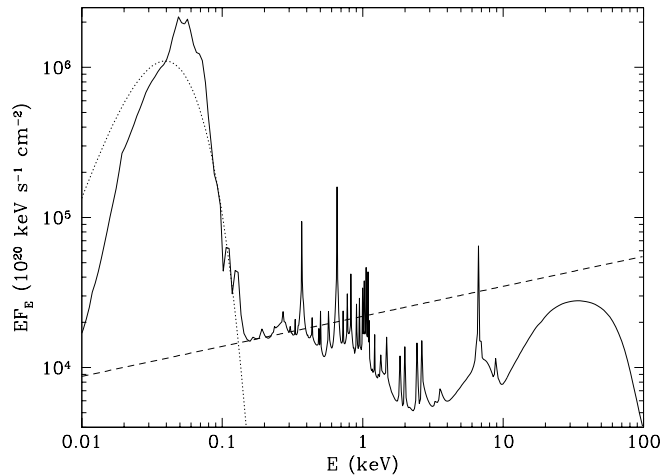


Figure 1. Computed reflection spectrum (solid line) with $\xi = 500 \text{ erg cm s}^{-1}$ and solar abundances. The incident $\Gamma = 1.8$ power-law and 10 eV blackbody are displayed as dashed and dotted lines, respectively. The power-law and reflection spectrum were added together prior to the equivalent width calculations.

appropriate fraction of emission-line photons that escape (in narrow profiles) directly from the gas without undergoing any further continuum absorption or Compton scattering is kept track of separately from the rest of the diffuse radiation originating within the gas (Ross 1979). Finally, the L shell lines of Fe XVII–XXII were changed from 3d→2p transitions to 3s→2p transitions. Like the other prominent lines, the Fe L-lines are produced by recombination. Liedahl et al. (1990) have pointed out that recombination cascades favour the production of 3s→2p lines over 3d→2p lines, and this effect is enhanced by resonance trapping of 3d→2p lines in optically thick gas. We assume that all recombinations to Fe XVII–XXII, except for radiative recombinations directly to the 2p level, ultimately result in 3s→2p emission.

The results of Ross & Fabian (1993) and Ross et al. (1999) have shown that, over a wide range of ξ , the Ly α line of O VIII is typically the strongest soft X-ray emission line in the reflection spectrum. Therefore, this is the line that is most likely to be detected by current instruments and so we computed models where it is expected to be at its most prominent. Specifically, reflection spectra were calculated for $\xi = 250, 500$ & $1000 \text{ erg cm s}^{-1}$. The incident spectrum was assumed to be a power-law with photon-index $\Gamma = 1.8$, typical of a Seyfert 1 galaxy (e.g., Nandra et al. 1997). Furthermore, a 10 eV blackbody illuminated the base of the slab (at a Thomson depth $\tau_T = 10$) with six times the flux of the power-law. An example of one of the computed spectra is shown in Figure 1. To investigate the effects of different metal abundances, a set of models was computed with five times the solar oxygen abundance, and another set with five times the solar nitrogen abundance. The initial set of abundances was taken from the list of Morrison & McCammon (1983).

The hydrostatic model requires many input parameters as the height of the disc at the irradiated point has to be explicitly calculated. For generality, we chose values typical of a Seyfert 1 galaxy: black hole mass $M = 10^7 M_\odot$, accretion rate $\dot{m} = 0.01$ (where $\dot{m} \equiv \dot{M}/\dot{M}_{\text{Edd}}$ and $\dot{M}_{\text{Edd}} = 48\pi M m_p G/\sigma_T c$, is the Eddington accretion rate), and the reflection occurs at a disc radius of 7 Schwarzschild radii. Radiation-pressure dominated boundary conditions were assumed. As with the constant density models, the sur-

face of the disc was illuminated with a $\Gamma = 1.8$ power-law, but with an incident-flux-to-disc-flux ratio $F_X/F_{\text{disc}} = 1$. These parameters resulted in a reflection spectrum similar to the $\xi = 500 \text{ erg cm s}^{-1}$ constant density model (see Sect 3.2) and thus isolates the differences due to the different density structures¹. Only a single model with solar abundances was computed with these parameters.

3 RESULTS

3.1 Constant density models

It is expected that for most Seyfert 1s, the X-ray power-law will be observed directly along with the reflection spectrum, so our analysis concentrates on the sum of the incident and reflection spectra (i.e., a reflection fraction of one). In Figure 2 we plot the resulting nine total spectra between 0.3 and 1.2 keV. The plots show many lines in this region of the spectrum which vary in shape and strength as the parameters are changed: C VI Ly α at 0.37 keV, N VI (resonance+intercombination) at 0.43 keV (usually very weak), N VII Ly α at 0.50 keV, O VII (resonance+intercombination) at 0.57 keV, O VIII Ly α at 0.65 keV, and a cluster of Fe L lines (particularly from Fe XVII–XIX) between ~ 0.7 and 1.0 keV. In Table 1 the equivalent widths (EWs) of the most prominent lines are listed for each of the nine models, as well as the width of their blue wings (WBW). The EWs were calculated by integrating the spectrum over the line between two hand-picked values of the continuum on either side. The WBW is simply the difference between the continuum on the high-energy side of the line and the value of the spectrum at the line peak, and is the minimum width of the line. Since the continuum can be difficult to determine at times (particularly in the cases with high O abundance), these measurements will not necessarily be very precise, but will accurately show trends in the data.

Concentrating on the models with solar abundances (the left-hand column in Fig. 2), we see that the O VIII line is the most prominent soft X-ray emission feature at all three ionization parameters with a maximum EW $\approx 73 \text{ eV}$ when $\xi = 250 \text{ erg cm s}^{-1}$. As ξ is increased to $1000 \text{ erg cm s}^{-1}$, the N and Fe L lines have all but disappeared, and the O VIII line is drastically weaker (EW $\sim 31 \text{ eV}$) with broad wings on either side of the line core due to Compton scattering (WBW $\sim 60 \text{ eV}$).

According to Table 1 all of the lines have a WBW on the order of tens of eV, even at lower ionization parameters. This is because the majority of the O VIII line emission occurs at a non-negligible Thomson depth and Compton scattering is a major contributor to the shape of the line. As an illustration, in Figure 3 the oxygen ionization fractions in the $\xi = 500 \text{ erg cm s}^{-1}$ model are plotted as functions of Thomson depth. In this case, large fractions of O VIII and O VII are produced only at Thomson depths $\gtrsim 1$. Therefore, the line emission from these species must pass through an optically thick scattering layer before escaping. As ξ increases the lines originate from a larger Thomson depth and the photons are scattered more often.

Increasing the O abundance by a factor of five primarily increases the strength of the O VII line. This is because the incident

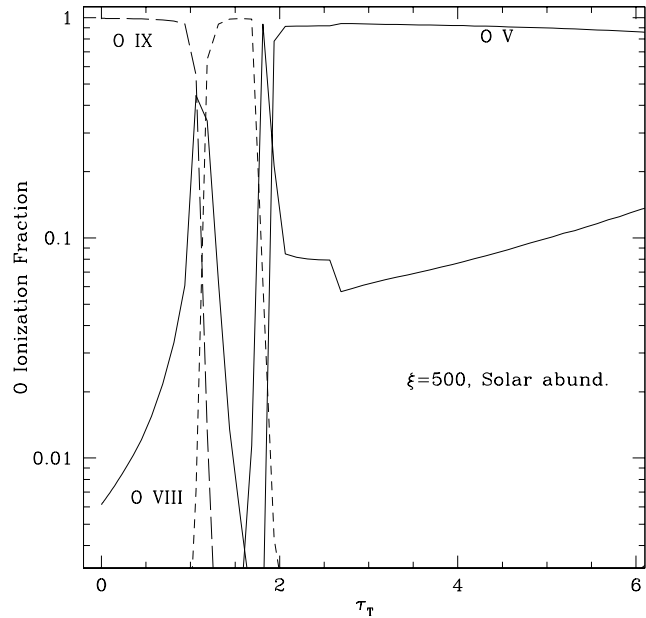


Figure 3. The oxygen ionization fractions for the $\xi = 500 \text{ erg cm s}^{-1}$, solar abundance model. The maximum production of O VIII Ly α occurs at a Thomson depth ~ 1 , so the line photons will likely be Compton scattered, thereby broadening the profile, as they pass through the surface of the slab.

spectrum is held constant and the number of possible ionizations from O VIII to O IX is fixed. With the increase in O abundance, it is no longer possible to fully-strip a large zone of O, and the curves seen in Fig. 3 are shifted to the left. Furthermore, since all of the ionizing photons have been used up, a larger number of oxygen ions can recombine to the O VII configuration. Therefore, the O VII line strongly increases with the oxygen abundance. In fact, at $\xi = 250 \text{ erg cm s}^{-1}$ the EWs of both the O VII and O VIII lines are $\sim 260 \text{ eV}$ which would hopefully be strong enough to be detected in a high signal-to-noise spectrum of a Seyfert 1.

In contrast to O, when N is increased by a factor of five, only the N VII line grows significantly. This is due to the fact that, even with a five times overabundance, N is not abundant enough for the N VII edge to saturate in these conditions. The N VII line is strongest in the $\xi = 250 \text{ erg cm s}^{-1}$ N-overabundant model, but still has an EW of only 21 eV. In all other cases, the EW of N VII is $\lesssim 20 \text{ eV}$. We conclude that at the current time it is unlikely for N VII Ly α emission to be observed from an irradiated accretion disc.

The C VI line is usually the second strongest line in the reflection spectrum with EWs between 10 and 30 eV. In the solar abundance model the C VI EW only decreases by about a factor of two as the ionization parameter is increased from $250 \text{ erg cm s}^{-1}$ to $1000 \text{ erg cm s}^{-1}$. These results certainly suggest that the C VI, O VII and O VIII lines are the best candidates for observable soft X-ray accretion disc lines.

3.2 Hydrostatic model

The summed reflection and incident spectrum from the hydrostatic model is shown in the left panel of Figure 4. Qualitatively, the spectrum looks similar to the $\xi = 500 \text{ erg cm s}^{-1}$ constant density model with O VIII Ly α dominating the emission. However, many of

¹ If $F_X/F_{\text{disc}} = 1/6$ rather than 1 for the hydrostatic model, the added Compton cooling decreases the Compton temperature and hence the effective ionization parameter of the atmosphere. The actual differences between these two reflection spectra in the energy range of interest are fairly small, with the most significant change being narrower lines due to the O emission region lying within 0.5 Thomson depths of the surface.

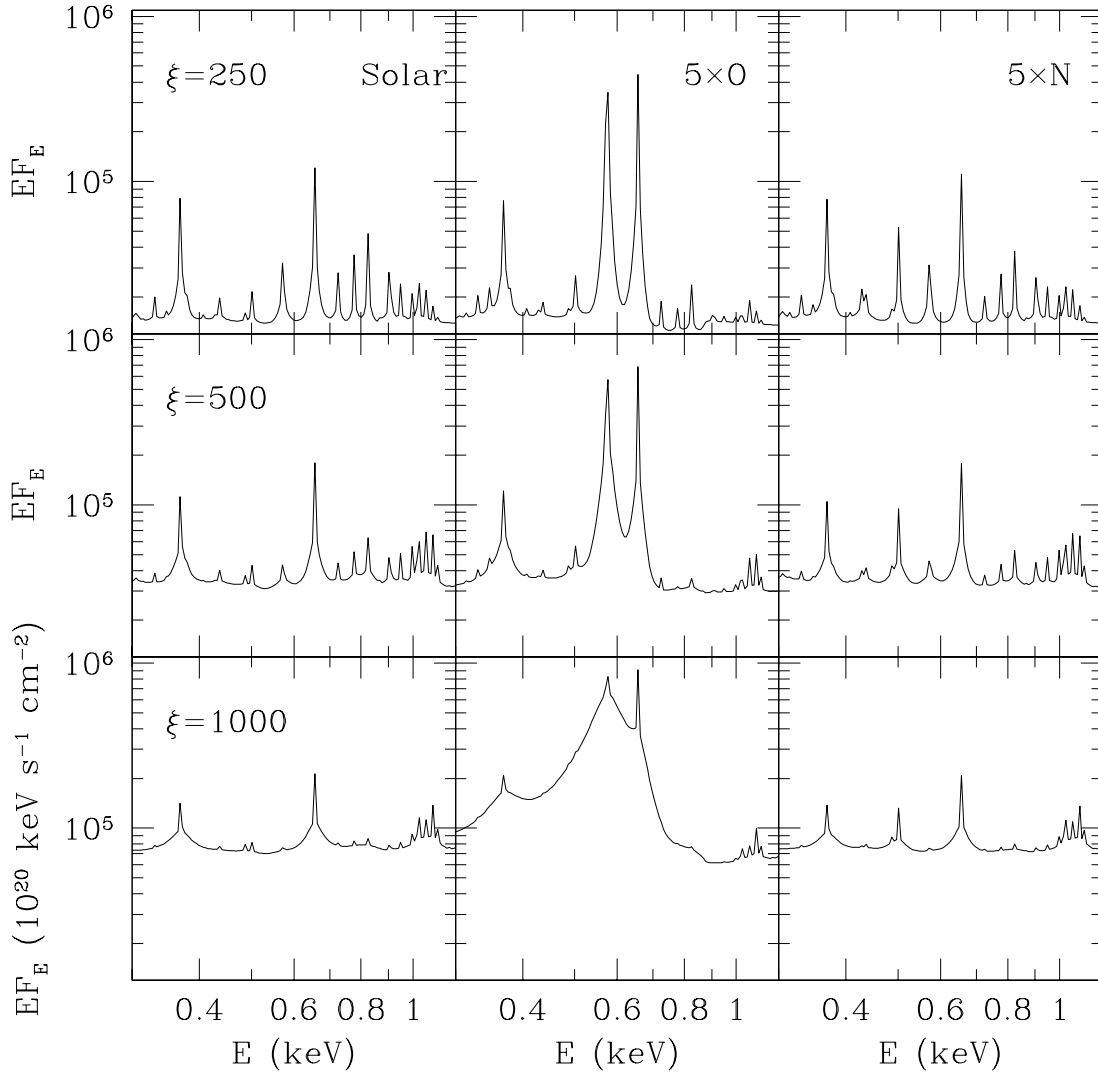


Figure 2. Total (reflected+incident) spectra between 0.3 and 1.2 keV calculated for $\xi = 250, 500$ & 1000 erg cm^{-1} and three different abundance sets (solar, 5 times the solar O abundance, and 5 times the solar N abundance). Each model included a 10 eV blackbody spectrum incident on the bottom of the slab with six times the flux of the irradiating power-law. The most prominent lines present in the spectra are, from left to right, C VI Ly α , N VI (resonance+intercombination; usually very weak), N VII Ly α , O VII (resonance+intercombination), O VIII Ly α , and a cluster of Fe L lines. As the ionization parameter of the slab is increased (moving downward in the plot), the emission lines weaken significantly because of the increased ionization level and are broadened due to Compton scattering. Increasing the oxygen abundance significantly strengthens the O VII line and distorts this part of the spectrum. A similar, but much less dramatic, effect is seen when the nitrogen abundance is increased. In this case, the N VII line is most affected, but the rest of the spectrum is relatively unchanged.

Table 1. Values of the emission line equivalent width (EW) and the width of the blue wing (WBW) for the spectra shown in Fig. 2. Both quantities are tabulated in eV. The WBW was defined simply as the difference between the base of the blueward wing and the peak of the line. In general, the EWs decrease as ξ is increased and the WBW are always on the order of tens of eV.

Line	Const. density with $\xi = 250 \text{ erg cm}^{-1}$						Const. density with $\xi = 500 \text{ erg cm}^{-1}$						Const. density with $\xi = 1000 \text{ erg cm}^{-1}$					
	Solar		5xO		5xN		Solar		5xO		5xN		Solar		5xO		5xN	
	EW	WBW	EW	WBW	EW	WBW	EW	WBW	EW	WBW	EW	WBW	EW	WBW	EW	WBW	EW	WBW
C VI	26	23	22	27	23	19	19	31	25	47	16	31	14	51	13	43	9.5	43
N VII	2.8	10	4.1	20	21	36	1.8	15	2.1	15	18	36	0.7	10	0.2	0	8.5	42
O VII	15	35	255	42	14	35	4.8	35	163	48	4.8	35	0.3	11	85	67	0.2	11
O VIII	73	40	256	40	66	40	51	54	130	62	51	47	31	62	19	62	29	62

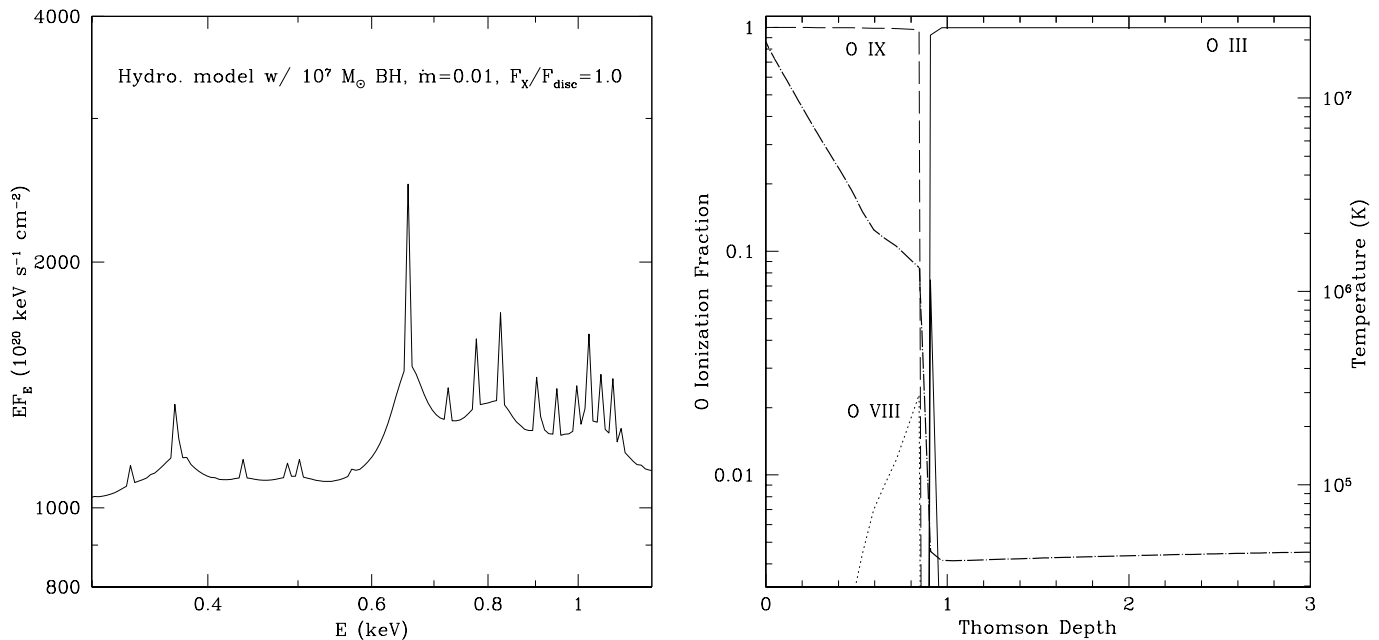


Figure 4. (Left) Total (reflected+incident) spectrum between 0.3 and 1.2 keV computed using a hydrostatic ionized disc model. The model assumed a gas-dominated accretion disc around a $10^7 M_{\odot}$ black hole accreting at 1 percent of its Eddington rate ($\dot{m}=0.01$). The illuminating flux was chosen to be equal to the disc flux. The spectrum is qualitatively similar to the $\xi = 500 \text{ erg cm s}^{-1}$ constant density model, but the lines are broader due to scattering by the hot, ionized skin found on the surface of the hydrostatic atmosphere. (Right) Oxygen ionization fractions for the hydrostatic model shown in the other panel. The gas temperature is also displayed as the bold dot-dashed line. The oxygen emission lines mostly originate at a Thomson depth of ~ 1 , but must traverse a hot, ionized layer before escaping. This ionized skin is common in hydrostatic models and results in broader emission lines than in the analogous constant density calculation.

Table 2. As in Table 1, but using the results of the hydrostatic model (Fig. 4). Both quantities are in units of eV. Although the spectrum is qualitatively similar to the $\xi = 500 \text{ erg cm s}^{-1}$ model, the lines are weaker and broader than those in the corresponding constant density spectrum.

Line	EW	WBW
C VI	3.1	43
N VII	0.27	15
O VII	0.10	11
O VIII	17	54

the lines have broader bases than in the analogous constant density spectrum. The broad bases are particularly apparent for the C VI (WBW=43 eV), and Fe L lines. Furthermore, as seen in Table 2, the lines are actually quite weak with the EW of O VIII only reaching 17 eV. These values are in good agreement with the results of similar computations done by Rózańska et al. (2002) and Nayakshin (private communication).

The reason for these differences is that the more realistic density structure results in a hot scattering layer overlying the line emitting material. In the right-hand panel of Figure 4 the vertical temperature profile of the hydrostatic model is overlaid on a plot of the oxygen ionization structure. We see that the temperature reaches $kT \sim 1 \text{ keV}$ at the surface of the atmosphere, which is nearly an order of magnitude hotter than the surface of the $\xi = 500 \text{ erg cm s}^{-1}$ constant density model. Oxygen is fully stripped until a Thomson depth of 0.9, where, because of the rapidly increasing gas density, it quickly recombines to O III, the lowest ionization state that is treated. Most of the O VIII emission therefore

originates from a narrow zone which is not very dense. Thus the O VIII line is intrinsically weaker in a hydrostatic disc model. The region in which large fractions of O VII–VIII are produced is so restricted that the O VII line is very much weaker in the hydrostatic model than in the constant density models. Therefore, the hydrostatic models predict that only O VIII is detectable.

The existence of the hot, fully ionized skin on the surface of the disc dilutes the spectral features which are formed underneath by Compton scattering the emission lines. This results in the broad bases seen in Figure 4. Although most of the O VIII emission originates from only a single Thomson depth into the atmosphere, the temperature of the ionized skin is such to result in significant dispersion. An ionized skin at the surface of the atmosphere is a common feature of hydrostatic disc models (Nayakshin et al. 2000; Ballantyne et al. 2001). If the illuminated hydrostatic models are a more realistic description of accretion discs than the constant density ones, then soft X-ray accretion disc lines are expected to be weak and broad features, and will therefore be challenging to detect.

4 DISCUSSION AND IMPLICATIONS

The ultimate goal of X-ray spectroscopy of AGN is to learn about accretion flows around supermassive black holes. Detecting soft X-ray emission lines from the accretion disc would complement the information inferred from the Fe $K\alpha$ line. In principle this should be relatively straightforward as the effective area of most X-ray detectors peak in the soft X-ray band, and gratings observations would allow an accurate determination of any warm absorber. Un-

fortunately, the calculations presented in the previous section suggest that most of the emission lines will be quite weak and broad (even before relativistic blurring), and therefore difficult to pull out of the noise with current instruments². The one exception may be the O VIII Ly α line which has an EW that can approach 100 eV, depending on the density structure of the disc. If that line could be measured accurately enough then, as seen in Fig. 2, it would give a good constraint on the ionization parameter of the disc. If significant O VII emission is also seen then abundance information may also be derived. Although the unambiguous detection of individual lines will likely be a challenge, soft X-ray accretion disc lines have the potential to be important to the study of AGN.

4.1 The soft X-ray features of MCG–6-30-15

Recently, Branduardi-Raymont et al. (2001) and Sako et al. (2002) claimed to have detected relativistically blurred C VI Ly α , N VII Ly α and O VIII Ly α lines in *XMM-Newton* RGS observations of the Seyfert 1 galaxies MCG–6-30-15 and Mrk 766. This interpretation was challenged by Lee et al. (2001) who favour a dusty warm absorber model to explain the features seen in their *Chandra* gratings data of MCG–6-30-15. The predictions of ionized disc models should be able to provide a data-independent view of which interpretation is most probable. Ballantyne & Fabian (2001) fitted the ionized disc models of Ross & Fabian (1993) and Ballantyne et al. (2001) to the *ASCA* data of MCG–6-30-15, concentrating on the region around the Fe K α line. The resulting best fit models predicted O VIII, O VII and Fe L emission with EWs < 20 eV, incompatible with the results of Branduardi-Raymont et al. (2001).

The results presented in Sect. 3 enable us to take an orthogonal point of view. Ignoring the Fe K α line entirely, we can ask the question: is there a region in the explored parameter space which can account for the putative soft X-ray emission lines? The updated analysis of MCG–6-30-15 by Sako et al. (2002) is very specific: they only see emission lines of O VIII, N VII and C VI with EWs of 162 ± 8 eV, 54.4 ± 3.2 eV and 24.9 ± 2.5 eV, respectively. From Table 1 it seems that a constant density model with $\xi = 250$ erg cm s⁻¹ and an O overabundance could account for the C and O lines, but none of the models can account for the strength of the N line, unless there is also a large (i.e., greater than 5 times solar) overabundance of N. However, these models predict significant O VII and Fe L emission which is not seen by Sako et al. (2002), although detectable given the limits placed on the other lines. The only way to remove these features would be to increase the ionization parameter, but this will weaken and smear out the O VIII line. Of course, it will be even more difficult to obtain the required line strengths with hydrostatic models because the emission features are intrinsically weaker.

Our calculations point to another serious problem with the relativistic emission line interpretation. Namely, the blue wing of the putative O VIII line is very sharp, dropping down at 700 eV to the continuum in $\Delta E \ll 10$ eV, as judged from the high resolution *Chandra* data where the drop is < 3 eV (Fig. 1 in Lee et al. 2001). The line must therefore have a relative width of much less than one per cent. Even a single scattering from an electron at 10^6 K will impart a rms width of 2 per cent to the line, rising to 6 per cent at

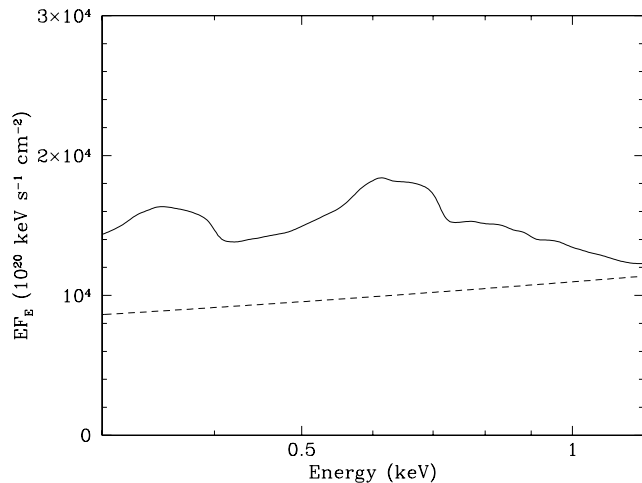


Figure 5. The $\xi = 250$ erg cm s⁻¹, solar abundance total (reflected+incident) spectrum between 0.3 and 1.2 keV blurred with the MCG–6-30-15 diskline parameters of Sako et al. (2002) ($i = 38.5$ degrees, $q = 4.49$, $r_{\text{in}} = 3.21 r_g$, and $r_{\text{out}} = 100 r_g$, where $-q$ is the radial emissivity power-law index, and $r_g = GM/c^2$). The dashed line shows the incident $\Gamma = 1.8$ power-law. The blue wing of the blurred oxygen lines extends over ~ 50 eV, as opposed to the < 3 eV drop measured by *Chandra* and *XMM-Newton*. The peak of the line now occurs at 0.6 keV.

10^7 K. A sharp observed feature from a line must therefore be due to the unscattered line core³, which usually carries little flux.

The ionized disc models predict a *minimum* width of the O VIII line of over 40 eV (Table 1). Relativistic blurring makes the width even larger. Figure 5 shows the results of blurring the $\xi = 250$ erg cm s⁻¹ solar abundance model (the top-left model from Fig. 2) with the parameters given by Sako et al. (2002). With the relativistic blurring effects, the O VII and O VIII lines are combined together and peaks at 0.6 keV. At 0.7 keV the blue wing of this blended line falls by only 20 per cent over a range of 50 eV. This is significantly weaker than the factor of 2–3 drop over ~ 3 eV seen in the *Chandra* and *XMM-Newton* data. The 0.7 keV drop is weaker in this reflection model because the Fe L lines have been blurred together and redshifted against the edge of the oxygen lines. The oxygen lines can be made sharper by moving to lower ξ , but only at the expense of increasing the strength of the O VII and Fe L lines. As before, hydrostatic models make the situation worse because they provide additional Compton scattering due to the ionized skin. Of course, these considerations also apply to Mrk 766.

Although we have obviously not covered the entire available parameter space, we conclude that it is very difficult, if not impossible, for reflection from ionized discs to produce the lines required by the interpretation of Branduardi-Raymont et al. (2001) and Sako et al. (2002). First, there does not seem to be a situation where one can obtain strong O VIII, N VII and C VI Ly α emission without simultaneously having significant O VII and Fe L lines. Second, in any situation where O VIII does dominate the emission spectrum, the disc has to be fairly highly ionized and so the lines are Compton broadened with widths of 10s of eV. This width will further increase upon relativistic blurring, and therefore cannot possibly have the sharp, $\ll 10$ eV drop at the high-energy side that the MCG–6-

² If, as the recent numerical simulations of Turner, Stone & Sano (2002) suggest, the disc is clumpy or inhomogeneous, then it is much more difficult to predict the properties of the reflection spectrum.

³ Broadening by electron scattering is relevant to all narrow emission lines produced by reflection, and could strongly modify predictions, e.g. those of Li, Gu & Kahn (2001).

30-15 data requires. More realistic hydrostatic ionized disc models exacerbate these problems because of the hot ionized skin on the surface of the disc. In general, any soft X-ray relativistic line will tend to create broad weak features in the observed spectrum. Any large sharp drops in this spectral range must be due to absorption edges.

It is likely there are weak broad features due to ionized oxygen in the spectrum of MCG-6-30-15. They are a plausible identification for the soft excess required in spectral modelling of *Chandra* data by Lee et al. (2001) and for the residuals from a dusty warm absorber fit to *XMM-Newton* data by Sako et al. (2002, see their Fig. 4). On the basis of our calculations, we conclude that the sharp drop seen in all soft X-ray spectra of MCG-6-30-15 at 0.7 keV cannot plausibly be the blue wing of an O VIII emission line produced by reflection.

ACKNOWLEDGEMENTS

The authors thank the referee, Masao Sako, for his helpful comments and suggestions. DRB acknowledges financial support from the Commonwealth Scholarship and Fellowship Plan and the Natural Sciences and Engineering Research Council of Canada. ACF and RRR acknowledge support from the Royal Society and the College of the Holy Cross, respectively.

REFERENCES

- Ballantyne D.R., Fabian A.C., 2001, MNRAS, 328, L11
 Ballantyne D.R., Ross R.R., 2002, MNRAS, 332, 777
 Ballantyne D.R., Ross R.R., Fabian A.C., 2001, MNRAS, 327, 10
 Branduardi-Raymont G., Sako M., Kahn S.M., Brinkman A.C., Kaastra J.S., Page M., 2001, A&A, 365, L140
 Fabian A.C., Rees M.J., Stella L., White N.E., 1989, MNRAS, 238, 729
 Fabian A.C., Iwasawa K., Reynolds C.S., Young A.J., 2000, PASP, 112, 1145
 George I.M., Fabian A.C., 1991, MNRAS, 249, 352
 Lee J.C., Ogle P.M., Canizares C.R., Marshall H.L., Schulz N.S., Morales R., Fabian A.C., Iwasawa K., 2001, ApJ, 554, L13
 Li Y., Gu M.F., Kahn S.M., 2001, ApJ, 560, 644
 Liedahl D.A., Kahn S.M., Osterheld A.L., Goldstein W.H., 1990, ApJ, 350, L37
 Magdziarz P. & Zdziarski A.A., 1995, MNRAS, 273, 837
 Matt G., Perola G.C., Piro L., 1991, A&A, 247, 25
 Morrison R. & McCammon D., 1983, ApJ, 270, 119
 Nandra K., George I.M., Mushotzky R.F., Turner T.J., Yaqoob T., 1997, ApJ, 477, 602
 Nayakshin S., Kazanas D., Kallman T., 2000, ApJ, 537, 833
 Pounds K.A., Nandra K., Stewart G.C., George I.M., Fabian A.C., 1990, Nature, 344, 132
 Ross R.R., 1979, ApJ, 233, 334
 Ross R.R., Fabian A.C., 1993, MNRAS, 261, 74
 Ross R.R., Fabian A.C., Young A.J., 1999, MNRAS, 306, 461
 Różańska A., Dumont A.-M., Czerny B., Collin S., 2002, MNRAS, 332, 799
 Sako M., et al., 2002, ApJ, submitted (astro-ph/0112436)
 Shakura N.L., Sunyaev R.A., 1973, A&A, 24, 337
 Tanaka Y., et al., 1995, Nature, 375, 659
 Turner N.J., Stone J.M., Sano T., 2002, ApJ, 566, 148
 Yaqoob T., Padmanabhan U., Dotani T., Nandra K., 2002, ApJ, 569, 487
 Życki P.T., Krolik J.H., Zdziarski A.A., Kallman T.R., 1994, ApJ, 437, 597

This paper has been typeset from a $\text{\TeX}/\text{\LaTeX}$ file prepared by the author.